Anti-icing performance and durability of suspension plasma sprayed TiO2 coatings4

Navid Sharifi, Ali Dolatabadi, Martin Pugh, Christian Moreau

PII: S0165-232X(18)30333-1
DOI: https://doi.org/10.1016/j.coldregions.2018.11.018
Reference: COLTEC 2702

To appear in: *Cold Regions Science and Technology*

Received date: 26 July 2018
Revised date: 24 November 2018
Accepted date: 30 November 2018

Please cite this article as: Navid Sharifi, Ali Dolatabadi, Martin Pugh, Christian Moreau , Anti-icing performance and durability of suspension plasma sprayed TiO2 coatings4. Coltec (2018), https://doi.org/10.1016/j.coldregions.2018.11.018

Anti-icing Performance and Durability of Suspension Plasma Sprayed TiO_2 Coatings4

Navid Sharifi[1], Ali Dolatabadi, Martin Pugh and Christian Moreau

Department of Mechanical, Industrial and Aerospace Engineering, Concordia University

1455 de Maisonneuve Blvd. W, Montreal, Quebec, Canada, H3G 1M8

[1] For review purposes and correspondence during the review process, please contact Navid Sharifi (navid.sharifi@concordia.ca, +1-514-994-2140). If the manuscript is accepted for publication, ultimately Professor Christian Moreau (christian.moreau@concordia.ca) will be the final and ultimate corresponding author.

Abstract

Superhydrophobic coatings are a potential solution for mitigating the in-flight icing problem for aircraft. However, to develop a superhydrophobic coating which can be practically used for aircraft and that possesses sufficient durability is an ongoing challenge. In this work, superhydrophobic coatings are developed using suspension plasma spraying (SPS) as a flexible, versatile and scalable coating technique. The anti-icing and deicing performances of these SPS coatings are studied in icing wind tunnel experiments. Furthermore, the durability of these SPS coatings is tested in dry particle and cloud-sized water droplet erosion and icing/deicing cyclic tests. The capability of SPS superhydrophobic coatings to reduce ice accretion is comparable to that of commercial superhydrophobic coatings but perform better in deicing tests using heating. Additionally, compared to commercial superhydrophobic coatings, the SPS coatings demonstrate significantly better performance in dry particle and icing/deicing cyclic tests while showing comparable durability in cloud-sized water droplet erosion tests. It is also shown that in case of high intensity water erosion, when the superhydrophobicity of SPS coatings deteriorates, it can be restored using a simple and quick retreatment process due to the robustness of the hierarchical micro-textured TiO_2 base coatings.

Key words: Superhydrophobic coating, Suspension plasma spray, Icing, Durability

1. Introduction

In-flight icing poses a major hazard to the safe and efficient operation of aircraft [1]. Ice accretion on various surfaces of aircraft causes an array of issues, including disturbance in aerodynamics, potential damage to external components and interference in the function of its sensors [2–4]. As a result, in-flight icing can cause a range of undesired consequences such as flight delays, emergency landings, damaged parts and increased energy consumption to deal with the icing problem [5]. The Federal Aviation Agency (FAA), have reported 319 icing-related accidents during the period of 1998-2007 [6]. Icing is estimated to cost around $96 million annually in terms of injuries and damage in the US only [7]. In addition, ice build-up on wind turbines and power lines due to super-cooled rain droplets can cause major problems [8,9].

In-flight icing occurs due to the presence of super-cooled water droplets i.e. water droplets with a temperature below their freezing point [10,11]. The accumulation of ice as a result of the impact of these droplets on the aircraft surfaces, progressively results in build-up of ice layers that can be as thick as several millimeters [12]. The rate and characteristics of the in-flight ice depend on a number of meteorological parameters. The first parameter is liquid water content (LWC) which is an indicator of the relative humidity in the cloud in terms of grams of water per cubic meter of air. The second parameter is the temperature of the ambient air and water droplets. The third parameter is the average size of water droplets in the cloud (this is expressed as median volumetric diameter-MVD). The typical icing risk conditions are reported in Table 1.

Table 1. Icing risk conditions [5].

Parameter	Icing risk conditions
Liquid water content (of water in air)	From 0.1 to 3 g/m^3
Temperature	From +4°C to -40°C
Droplet diameter (MVD)	Usually from 1-50 μm but also up to 400 μm

In-flight ice is often categorized into two distinct types [13]. The first type is called glaze or clear ice and typically forms at temperatures close to 0°C when the water droplets do not immediately freeze upon impact but run back and shed on the surface which results in a glassy, transparent, relatively smooth and dense ice. The second type of ice is called rime ice and forms at lower temperatures (typically -10°C and lower) when super-cooled water droplets freeze upon impact with the substrate, creating a white, irregular ice. Out of these two types, glaze ice is considered to be potentially more dangerous due to its high adhesion and the fact that it can form on various regions of the surface rather than only the point of impact [14].

Various methods have been employed to deal with the icing problem including good weather forecasting, pilot training, optical ice detection systems and computer simulations [15]. Additionally, in-flight anti-icing and deicing systems based on heating or mechanical ice removal have been developed [16–18]. This approach can be effective in preventing ice accumulation on the leading edge. However, it is impractical to place heating elements or vibrators below all surfaces that are prone to icing on an aircraft. Therefore, efforts have been focused on using superhydrophobic coatings to prevent or delay ice formation or to reduce ice

adhesion, in order to improve the efficiency of thermal and mechanical anti-icing and deicing systems [19–21].

Superhydrophobic coatings are surfaces with both high water repellency, manifested through water contact angles of greater than 150°, and high water mobility, manifested through contact angle hysteresis and/or sliding angles lower than 10° [22]. The extreme water repelling characteristic of a superhydrophobic surface is due to the combination of a relatively low surface energy and the presence of a hierarchical micro-texture i.e. a surface texture with both micron-sized and nano-sized roughness [23]. Superhydrophobic surfaces have found potential applications where minimal interaction of a solid surface and a liquid is desired such as anti-icing [24], anti-corrosion [25], drag-reduction [26] and drop-wise condensation [27].

Studies have shown that ice formation can be efficiently delayed or even in certain conditions completely prevented on superhydrophobic surfaces [28–30]. This is because super-cooled water droplets do not easily stick on a superhydrophobic surface and mainly bounce off and detach from it before freezing begins. The anti-icing capability of superhydrophobic surfaces, especially in the early stages of ice formation, is demonstrated frequently by comparing the onset of ice nucleation on superhydrophobic and non-superhydrophobic surfaces. However, some such icing experiments have been performed using relatively large and static water droplets [31,32] that do not necessarily represent in-flight icing conditions which involves water micro-droplets impinging on the surface with relatively high velocity.

Furthermore, some studies have claimed that ice adhesion can be significantly reduced on superhydrophobic surfaces due to the formation of air pockets between the solid surface and ice [8,33,34]. However, on the contrary, some other studies have reported an increase in ice adhesion due to the surface roughness which form a mechanical interlock with the ice [8,35].

These seemingly contradictory observations signify the importance of testing anti-icing performance of each novel superhydrophobic surface in icing conditions simulated in icing wind tunnels to resemble actual in-flight icing conditions.

Another major challenge in developing new superhydrophobic coatings for anti-icing applications is their mechanical durability. Common low-surface-energy materials used to develop superhydrophobic coatings are organic or polymeric materials which typically suffer from poor mechanical durability, especially in terms of erosion resistance. Therefore, considerable efforts have been focused on developing techniques and tests to improve, quantify and compare durability of superhydrophobic coatings [36,37]. Consequently, it is crucial for all new superhydrophobic coatings developed using various surface engineering techniques to be tested for different aspects of mechanical durability such as water erosion, sand erosion and icing/deicing cycles.

As a flexible (in terms of the variety of materials that can be deposited), versatile and scalable coating technique, thermal spraying has been employed to develop superhydrophobic and icephobic coatings. Juuti et al. [38] used a liquid precursor fed oxygen-hydrogen flame spray to deposit a porous titania layer which was then infused with silicone oil as lubricant to create a slippery surface. They showed that ice adhesion on such surfaces can be reduced by an order of magnitude which also facilitates deicing. In another work, Koivuluoto et al. [39] deposited polyethylene-based polymer coatings using flame spray and showed that the ice adhesion of these surfaces is significantly lower than metallic aluminum.

Recently suspension plasma spray (SPS) has been employed by the authors to develop superhydrophobic TiO_2 coatings [40]. In addition, the SPS process has been optimized [41] to achieve very high water repellency and mobility. These coatings have shown water contact

angles greater than 165°, water sliding angles as low as 1° and water contact angle hysteresis as low as 3°. In this work, the best samples of these SPS coating have been selected and investigated for their icing performance and durability. Results are then compared to commercially available polymer-based superhydrophobic spray-on coatings in order to better demonstrate the characteristics of the SPS superhydrophobic coatings.

2. Methodology

In this section, the coating deposition technique is briefly explained (more detailed explanations can be found in previous publications [40,41]), followed by two groups of tests designed to evaluate the icing performance and durability of the SPS TiO_2 superhydrophobic coatings.

2.1. Coating Fabrication

Coating samples were prepared using suspension plasma spraying of a titanium dioxide suspension feedstock onto 3 × 12 × 120 mm, grinded 304 stainless steel substrates (McMaster-Carr, Aurora, OH, USA). The feedstock suspension was prepared by mixing 10 wt% of titanium dioxide submicron sized particles with a nominal average particle size of 500 µm (TKB Trading, Oakland, CA, USA) into a solvent composed of a mixture of ethanol (Fisher Scientific, Ottawa, ON, Canada) and ethylene glycol (Fisher Scientific, Ottawa, ON, Canada) with a weight ratio of 4 to 1. Polyvinylpyrrolidone (PVP360, Sigma-Aldrich, Oakville, ON, Canada) was used as a dispersing agent in the suspension. Prior to deposition, the stainless steel substrates were grit-blasted for cleaning and to increase coating adhesion. A radial injection plasma torch (3MB, Oerlikon Metco, Pfäffikon, Switzerland) was used with a mixture of argon and hydrogen as plasma gas. The total plasma gas flow rate was 60 l/min. The power of the plasma was set to 36 kW by fixing the plasma current to 600 A, and adjusting the hydrogen flow rate so that the

plasma power was 60 V. During the deposition, the plasma torch stand-off distance was 5 cm and the suspension feed rate was 55 g/min. The plasma torch had a lateral speed of 1 m/s and a raster pattern with an overlap distance of 3 mm was used for deposition. After coating, the samples were cleaned with compressed dry air, decontaminated in boiling water and then isopropyl alcohol (Fisher Scientific, Ottawa, ON, Canada) and finally treated by dipping in a 0.5 % solution of stearic acid (Fisher Scientific, Ottawa, ON, Canada) in 1-propanol (Fisher Scientific, Ottawa, ON, Canada) and left at room temperature to dry. The 1-propanol was selected due to relatively high solubility of stearic acid in it and its availability. A more detailed description of the development of these superhydrophobic titanium dioxide coatings and optimization of the process to achieve the high water repellency and mobility can be found in the authors' previous articles [41]. The SPS TiO_2 superhydrophobic samples are denoted as "SPS" throughout this paper.

For comparison purposes, two commercial superhydrophobic products, NeverWet® (Rust-Oleum, Concord, ON, Canada) and Ultra-Ever Dry® (Ultratech International, Jacksonville, FL, USA) were used. These samples are denoted as "NW" and "UED" respectively throughout this article. Coatings were prepared on substrates similar to those used for preparation of SPS coatings and according to the manufacturer instructions. These additional samples were tested in the same conditions as SPS coatings to compare durability and performance.

2.2. Icing Tests

Two groups of tests were used to evaluate the different superhydrophobic coatings. The first group of tests were designed to evaluate the icing performance of the samples and included ice accretion and heated deicing tests. The second group of tests were designed to evaluate the durability of the coatings. They included dry particle erosion, cloud-sized droplet erosion, high

intensity water erosion and icing/deicing cyclic tests. All icing tests and droplet erosion and icing/deicing cyclic durability tests were carried out using an in-house developed closed loop icing wind tunnel at Concordia University. A schematic of the icing wind tunnel is shown in Figure 1. The test section of the wind tunnel has a square-shaped cross section with a width of 10 cm. The air velocity in the test section can reach a maximum of 45 m/s and the temperature of the air in the test section can be reduced to a minimum of -20°C with an air velocity of approximately 10 m/s. It is important to note that the minimum operating temperature of the wind tunnel increases with increasing air velocity due to the decreased residence time of air in the chiller. The liquid water content in the test section can be varied between 0.2-1 g/m^3.

Typically, aircraft velocity while flying through the clouds, where there is a risk of in-flight icing, is considerably lower than cruising speed and is close to 100 m/s [42]. Therefore, the maximum air velocity of 45 m/s in the icing wind tunnel presents a limitation. This is not a critical limitation in the icing tests where the goal is to study the effect of superhydrophobic coatings in mitigating ice accretion and comparing it to other commercially available superhydrophobic coatings as well as an uncoated surface. However, the limit in air speed in the wind tunnel can negatively affect the results of cloud-size water droplet erosion tests as the erosion due to the impact of droplets is proportional to their size and velocity. Thus, in order to compensate for the limited air speed, in the cloud-size water droplet erosion test, water droplets with sizes three times larger than what is typically expected in icing conditions are used. This is discussed in details in section 2.3.2 of this manuscript.

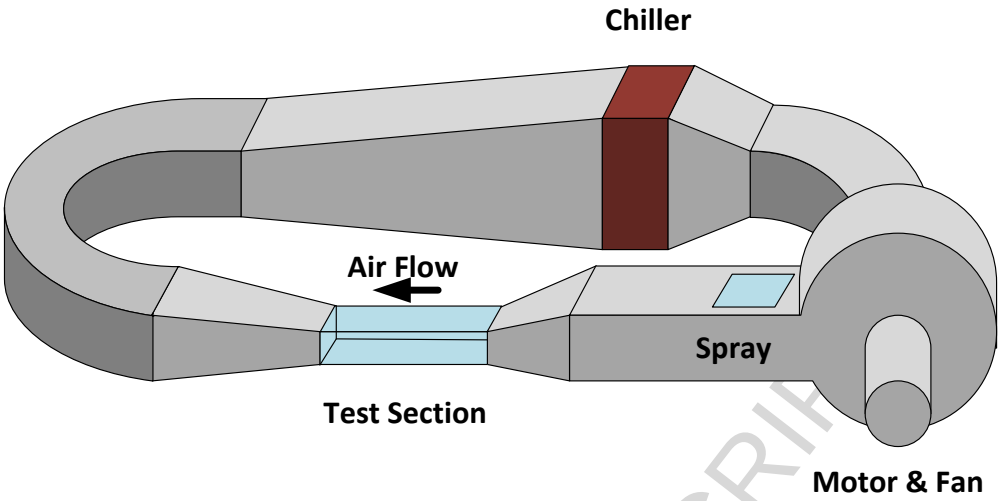

Figure 1. Schematic of the icing wind tunnel.

The water droplets were injected into the air stream using an air atomizing spray nozzle placed after the fan. The size distribution and spray pattern can be adjusted using the air flow and water flow controllers. The spray of droplets in the test section was characterized using a phase Doppler particle analyzer (PDPA), and in all the tests performed, the spray had an LWC of 0.5 g/m^3 with a median volume diameter (MVD) of 30 μm [43]. The LWC of the wind tunnel in testing condition was measured using an icing blade technique, recommended by SAE International in the "Aerospace Recommended Practice (ARP5905) Calibration and Acceptance of Icing Wind Tunnels". This method involves inserting a standard icing blade in the center of the test section and exposing it to the spray and accreting ice. The LWC can then be calculated by measuring the thickness of ice that has formed on the blade in a certain amount of exposure time. For the spray, cold distilled water was used. For icing tests the water was maintained below 4°C to ensure super-cooled water droplets reach the test section. The placement of the spray nozzle at 1.14 m upstream ensured that the water droplets in the test section had approximately the same velocity and temperature as the air stream. Furthermore, the air stream

velocity was measured using a Pitot tube probe and compared to the velocity of particles measure by PDPA to ensure that they were within 5% difference of each other.

A schematic of the sample holder that was used in the icing wind tunnel for icing and water droplet impact tests is shown in Figure 2. The flexible heater (KHLV-0504/10-P, St-Eustache, QC, Canada) shown in this schematic was used in the heated deicing tests. The details of these tests are discussed in the following sections.

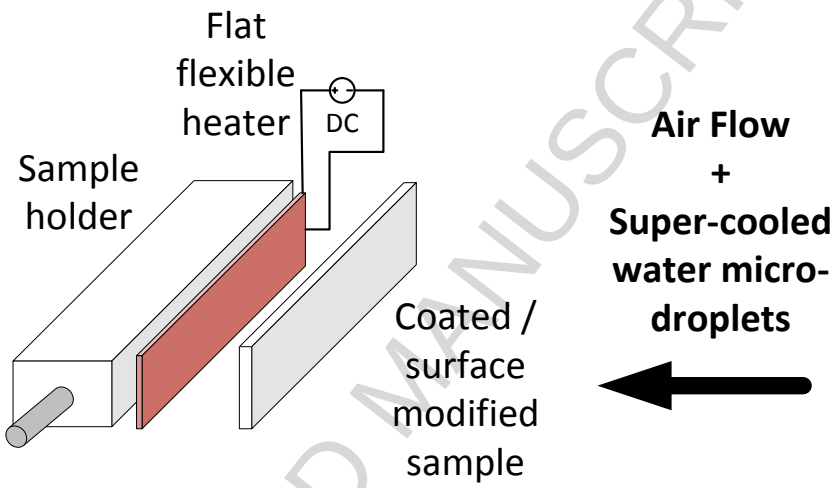

Figure 2. Schematic of the sample holder used in the wind tunnel for icing and water droplet impact tests.

2.2.1. Ice Accretion Test

Multiple sets of operating conditions were designed to represent various in-flight icing scenarios within the capabilities of the testing equipment. In all these conditions, the liquid water content (LWC) and median volume diameter (MVD) were 0.5 g/m^3 and 30 µm, respectively which correspond to the icing risk conditions presented in Table 1. In the case of air stream velocity, two values were selected, one being the maximum capacity of the wind tunnel i.e. 45 m/s and the other one corresponding to a motor frequency of half of maximum power which gave 25 m/s. It is important to note that by increasing the air stream velocity, the water input was

adjusted to ensure that the LWC value remained constant for all tests. In terms of temperature, two temperatures were selected, one slightly below the freezing temperature of water i.e. -3±1°C which typically results in formation of clear ice. The other temperature was -10±1°C which was the maximum cooling capacity of the chiller at an air velocity of 45 m/s and typically causes the formation of a mixture of glaze and rime ice which is typically referred to as "mixed ice". Except at the stagnation point/region, the impact of super-cooled water droplets on aerodynamic surfaces of aircraft is not perpendicular, therefore, samples were tested with both 90° and 45° angle of impacts to better represent the various surfaces of an aircraft. In order to better assess the delay in ice formation, the duration of each ice accretion test was 1 minute. The coupons were carefully weighed before and after each test to determine the weight of ice formed during the test. Each test was repeated 9 times for each sample and in order to minimize melting of ice during the measurement after icing, the sample were not handled by hand but using a pair of tweezers and the measurement was done immediately.

Table 2. The wind tunnel operating condition.

Variable	**Value(s)**
Air stream velocity (m/s)	23 and 45
Air stream temperature (°C)	-3 and -10
Angle of impact [AoI] (°)	45 and 90
LWC (g/m^3)	0.5
MVD of water droplets (μm)	30

2.2.2. Heated Deicing Tests

To evaluate the potential contribution of superhydrophobic coatings to the deicing process using heating, a flexible flat heating element was placed under the coupons (Figure 2). Then each sample was exposed to the harshest icing condition given in Table 2 for 1 minute. Then the spray was stopped while the rest of the operating parameters were kept constant. Then the sample was turned 45° so that the surface of the sample was at a diagonal with respect to the direction of the air stream before heating began. This step was necessary because if the sample was left perpendicular to the air direction, after heating the ice that is in direct contact with the substrate would melt, causing a gap between the remainder of the ice and the substrate surface which resulted in the layer of ice remaining intact. The heater under the sample was turned on with 24 W electrical power. The time necessary for complete ice removal was measured as the deicing time. It is important to note that in some cases, complete ice removal meant that the ice was completely melted, and in some cases after melting the layer close to the substrate surface, the remainder of ice would fly away from the test coupon. Both these conditions were accepted as the ultimate condition of ice removal.

For any icing condition, if enough heat input is given to the substrate, it is possible to maintain its surface free of ice. Consequently, another test was designed to measure the heat input required to maintain an ice-free surface. In this test, similar to the deicing test, a heater was positioned under the samples and they were fixed in the wind tunnel with the water spray closed. The heater was turned on and enough time was given for the temperature profile to reach steady state. The steady state was ensured by placing a small thermocouple under the samples, between the heater and the samples. When this thermocouple showed a constant temperature i.e. steady state condition was achieved, the spray was started. If ice started to form on the surface of the sample, the test was stopped, the sample was deiced, dried and the test was repeated with a heat

input 1 W higher than the previous run. If no ice had formed on the sample, the same process was repeated with a 1 W decrease in heating. Using a trial and error method, the minimum electrical power required to maintain an ice-free surface was measured and reported for each coating as well as for an uncoated sample.

2.3. Durability Tests

Four different tests were used to evaluate the durability of the superhydrophobic coating including dry particle erosion, cloud-sized water droplet erosion, high intensity water erosion and icing/deicing cyclic tests. These tests were designed to measure the deterioration of superhydrophobic behavior of the coatings after being exposed to erosive and destructive factors. The superhydrophobicity of samples was evaluated based on measurement of static contact angle (CA), contact angle hysteresis (CAH) and sliding angle (SA) of water on the surface. These wetting characteristics were each measured using an in-house setup, using a camera, a tilting surface which could be tilted with the precision of 1° and an automatic droplet dispenser. The CA and SA were measured using a 10 µL droplet of distilled and deionized water. For measuring advancing and receding contact angles (ACA and RCA respectively), an inflating/deflating droplet technique was used with the size of the droplet changing between 5 and 10 µL. The CAH was calculated as the difference between ACA and RCA values. An open source plug-in [44,45] to the image analysis software ImageJ was used to analyze the images and determine the contact angles.

2.3.1. Dry Particles Erosion Test

For evaluating the resistance of superhydrophobic coatings to solid particle erosion, a technique which is frequently used in literature [36,37,46–48] was employed. In this test, a fixed amount of abrasive particles, in this case 5 g of aluminum oxide particles (particle size of 37-149

μm) (635135, Canablast, Laval, QC, Canada) was poured onto the surface of the coatings from a fixed distance of 30 cm. The samples were placed at a 45° angle with respect to falling particles to ensure that particles move away from the point of impact. Erosion occurs due to the impact of falling particles accelerated only due to gravity. Afterwards, the surface of the samples was cleaned using compressed air and CA, CAH and SA of the samples were measured. This cycle was repeated 5 times for each sample.

2.3.2. Cloud-Sized Water Droplet Erosion Test

To evaluate the resistance of coatings to water droplet impact, similar to what happens in flight conditions, the samples were exposed to a spray of cloud-sized droplets inside the wind tunnel. This test was performed at room temperature with an air stream velocity of 45 m/s and a droplet MVD of 150 μm with a perpendicular angle of impact for a duration of 5 minutes for each cycle. It must be noted that the 150 μm droplet size used in this test is considerably higher than the cloud droplet size (typically MVD = 1-50 μm). This droplet size was selected to reduce test times since it would take a long time for 50 μm droplets to cause noticeable deterioration. After each cycle, the samples were removed from the test section, dried using compressed air and CA, CAH and SA of the coatings were measured and reported.

2.3.3. High Intensity Water Erosion Test

A high intensity water erosion rig with a rotating disk was used for this test. This rig which is one-of-a-kind testing apparatus was originally designed for testing erosion resistant coatings according to ASTM G73 standard [49,50]. The resulting erosion aggressiveness is far more severe than water erosion conditions encountered in flight conditions. Indeed, water erosion rate is directly proportional to the mass and velocity of impacting water droplets [51]. In this work, the water erosion rig was used at its least intense setting with water droplets with an

average diameter of 260 μm and impact velocity of 200 m/s. For an aircraft flying though clouds, which typically happens after takeoff and before landing, the speed is between 80-120 m/s and the droplet size in clouds is typically 5 – 50 μm [52]. Therefore, the kinetic energy of water droplets upon impact is at approximately three orders of magnitude higher in this test compared to in-flight conditions. However, it must be noted that an aircraft sometimes needs to fly though rain droplets which are larger than cloud-sized droplets but their impact on the surfaces of aircraft occurs with smaller velocities. Therefore, it is reasonable to assume that the type of erosion occurring during this high intensity water erosion test can be of the similar magnitude to the erosion from raindrops due to similar impact energy. Additionally, this test can be seen as an accelerated indicator of durability of superhydrophobic surfaces exposed to water droplet erosion. The minimum duration of the test with repeatable and consistent conditions was 5 seconds but the test was repeated for durations of 10, 20, 60, 300 and 12000 seconds as long as the coatings survived. After exposing the samples to this test, the samples were visually inspected and the wetting behavior of the samples was tested. Finally, micrographs of the eroded regions were prepared using SEM to study the wear damage.

2.3.4. Icing/Deicing Cyclic Test

To evaluate the durability of the coatings exposed to repetitive icing/deicing cycles, only the harshest icing condition i.e. highest air velocity and 90° angle of impact at -10°C was selected. The samples were exposed to this condition for a duration of 1 min, removed from the test section and then heated using a heat gun until the ice was fully molten. The samples were then dried using compressed air, and the SCA, CAH and SA of the samples were measured. This cycle was repeated multiple times for each sample. The total number of icing/deicing cycles was selected individually for each sample based on the observed changes in their corresponding

wetting properties. It is important to note that the 1 minute duration of the test was selected due to the fact that any longer duration for each run was not expected to have a significant effect because as soon as a complete layer of ice forms on the surface, the impinging droplets will impact on the ice layer rather than the actual surface of the samples.

3. Results and Discussion

After measuring the "as-prepared" wetting behavior, SEM micrographs of the SPS and commercial spray-on coatings were obtained and presented in Figure 3. A very distinct difference between the surface micro-texture of the SPS coating in comparison to the commercial polymeric coatings can be observed. In Figure 3 (a) and (b), it is demonstrated that the superhydrophobic SPS coating has a hierarchical surface micro-texture which, in combination with the surface treatment for lowering the surface energy, results in superhydrophobic behavior of this type of coating. It has been demonstrated in previous works [40,41] that SPS coatings without the hierarchical micro-texture do not demonstrate the same extreme water repelling behavior as hierarchically micro-textured coatings. On the other hand, the commercial coatings have a single scale surface roughness as demonstrated in Figure 3 (c) and (d). As a result, these coatings mainly depend on their surface chemistry with very low surface energy to deliver the superhydrophobic behavior. Additionally, it is noteworthy that in the case of the two commercial coatings, some micro-cracks can be observed in the coatings that are the result of the drying process and may influence mechanical integrity of the coating in icing conditions.

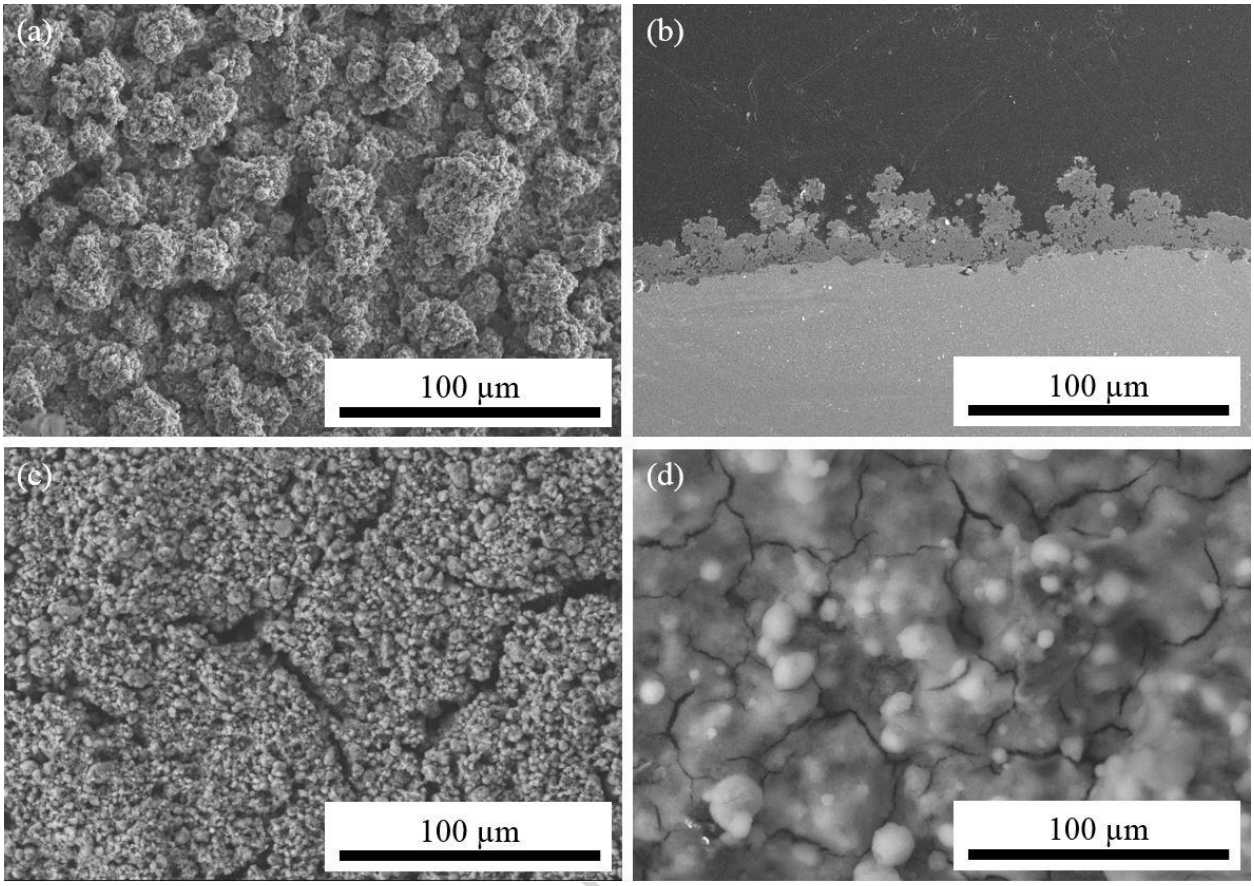

Figure 3. SEM micrographs of: (a) top and (b) cross-section of SPS coating; (c) UlterEver Dry coating; and (d) NeverWet coating.

3.1. Icing Tests

3.1.1. Ice Accretion Test

To evaluate the icing performance of the SPS superhydrophobic coatings in various conditions, a total of eight sets of icing parameters were selected as explained in the experimental section. For each set of icing conditions, the experiment was carried out nine times and the average value for ice accretion in terms of mass of ice is reported. The results for each case are compared to the results for an uncoated substrate. The ice accretion test results, reported in Table 3 show that the SPS superhydrophobic coating decreases the amount of accumulated ice in all tested icing conditions by providing delay in the ice formation. The reduction of ice

accretion ranges from 13 to 62 percent depending on the conditions. The highest decrease is observed for 23 m/s (lower) air velocity, -3°C (higher) temperature and an angle of impact of 45° which corresponds to glaze ice formation. This is expected as in temperatures closer to the freezing point, there is less chance of water droplets freezing immediately upon impact and the 45° angle of impact facilitates the removal of droplets by the oncoming air flow (similar to the majority of aerodynamic surfaces of aircrafts).

In general, according to Table 3, the effect of a superhydrophobic coating on decreasing ice accretion is more pronounced at -3°C when glaze ice typically forms compared to -10°C when mixed ice typically forms. This is because droplets with a relatively higher temperature stay liquid for a longer time and there is more chance of them being removed by the air stream due to the superhydrophobic behavior of the coating. This is potentially a benefit since as was mentioned in the introduction, glaze ice is typically considered to be more hazardous compared to rime and mixed ice.

Furthermore, according to Table 3, the decrease in ice accretion is larger for all cases when impact occurred at 45° compared to 90°. This is expected as the tilted surface allows more efficient removal of water droplets by the air stream and reduces freezing on the surface. At this point it should be noted that aircraft surfaces are normally curved and normal impact occurs around the stagnation point. Therefore the 90° angle of impact can be considered the worst-case scenario. It is reasonable to expect a more efficient decrease in icing for an aerodynamic shape such as an airfoil [43].

Table 3. Ice accretion test results. For all conditions, LWC = 0.5 g/m^3, MVD = 30 μm and test duration was 60 s. [St. Dev. = standard deviation; Est. Unc. = estimated uncertainty calculated using the root of the sum of the squares RSS]

Condition	Air Stream Velocity (m/s)	Air Stream Temperature (°C)	Angle of impact (°)	Type of ice	Ice accretion on uncoated sample (g) [± St. Dev.]	Ice accretion on SPS sample (g) [±St. Dev.]	Icing decrease (%) [±Est. Unc.]
1	23	-3	45	Glaze	0.98 ±0.02	0.37 ±0.04	62 ±5
2	23	-3	90	Glaze	0.96 ±0.02	0.49 ±0.02	49 ±3
3	23	-10	45	Mixed	1.12 ±0.02	0.51 ±0.02	54 ±3
4	23	-10	90	Mixed	1.3 ±0.02	0.87 ±0.03	33 ±4
5	45	-3	45	Glaze	0.97 ±0.02	0.43 ±0.03	55 ±4
6	45	-3	90	Glaze	1.11 ±0.03	0.54 ±0.02	51 ±4
7	45	-10	45	Mixed	1.49 ±0.02	0.84 ±0.02	43 ±3
8	45	-10	90	Mixed	1.83 ±0.04	1.58 ±0.04	13 ±9

The effect of air stream velocity is more complex than the previous two parameters. Since doubling the air stream velocity value while keeping all other parameters constant means that the number of droplets coming towards the surface has also doubled; one might expect to observe a significant increase in ice accretion. However, this is not the case according to Table 3. For both uncoated and coated samples, the increase in the mass of ice for doubling the air velocity is relatively small and in a couple of cases this increase is negligible. To explain this observation, it is necessary to consider the aerodynamic characteristics of the test section and the

samples. Since the samples in this test are all flat, in the case of 90° angle of impact, a strong stagnation region in the air flow is created. In both 45° and 90° angle of impact conditions, all droplets coming towards the surface of the samples do not necessarily impact on the surface and a number of them, especially the smaller droplets, are deviated by the air flow going around the sample. Increasing the velocity of the air stream can amplify this phenomenon which can explain why the ice accretion is not significantly increased by doubling the air stream velocity.

To compare the effect of the SPS superhydrophobic coating on decreasing icing with commercial superhydrophobic coatings, samples of the two commercial coatings were prepared and tested in two icing conditions (Conditions 1 and 8 in Table 3). The results are compared with the uncoated sample in Figure 4. This figure shows that, in these two icing conditions, all three superhydrophobic coatings decrease the ice accretion. The SPS coating shows slightly better performance in Condition 1 whereas, in Condition 8 the inverse is observed but the difference between the three coatings is smaller.

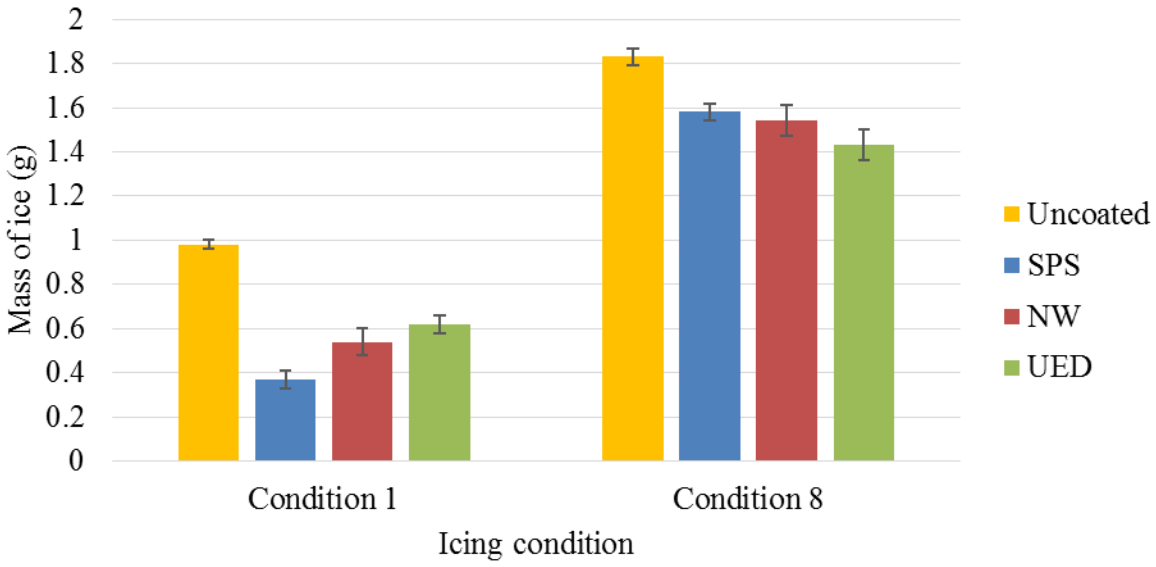

Figure 4. Ice accretion test comparison for uncoated sample versus the SPS, and the two commercial (NW and UED) coatings. (The error bars represent standard deviation)

3.1.2. Heated Deicing Tests

To study the effect of superhydrophobic coating on deicing time using heating, the three superhydrophobic coatings were put in icing Condition 8 for one minute. Afterwards, the water spray was stopped, and the sample was tilted to a 45° angle relative to the air stream. The electrical heating element underneath the sample was then turn on to a power of 24 W. The time for the samples to become completely ice-free was measured and is reported in Table 4. For all three superhydrophobic coatings, the deicing time was significantly shorter than that of the uncoated sample. One important observation is that for the three superhydrophobic surfaces, the ice-free surface was achieved due to detachment of the ice at some point after heating started, but for the uncoated sample, the ice-free surface was achieved by melting all the ice on the surface. Furthermore, the SPS superhydrophobic coating demonstrated the shortest deicing time compared to the other two commercial coatings. This can be attributed to the fact that the commercial coating are several hundreds of micrometers thick layers of polymer that act as a thermal insulator, delaying the heating of the interface of ice and sample. The SPS coating is only 10-20 μm thick. The thermal conductivity of non-porous TiO_2 is around 6.5 W/(mK) [53] at room temperature. For porous suspension plasma sprayed coatings, thermal conductivity can decrease by 10 to 50 percent depending on the porosity [54]. The exact value of the thermal conductivity for the commercial polymer coatings is unclear but for most polymers the thermal conductivity is considerably lower, rarely exceeding 0.5 W/(mK) [55]. In addition, the commercial polymer coatings are at least an order of magnitude thicker than the SPS TiO_2 coatings. Therefore, the thin SPS coating is not a significant barrier to heating the interface and therefore deicing is faster for it.

Table 4. Deicing time of each sample for 24 W heating power. [St. Dev. = standard deviation; Est. Unc. = estimated uncertainty calculated using the root of the sum of the squares RSS]

Sample	**Deicing time (s) [± St. Dev.]**	**Improvement (%) [± Est. Unc.]**
Uncoated	173 ± 8	--
SPS	34 ± 4	80 ± 5
NW	58 ± 3	66 ± 5
UED	47 ± 3	73 ± 5

To further study the effect of a superhydrophobic surface on deicing, another experiment was designed to determine the minimum electrical power required to maintain an ice-free surface for various samples. This experiment was performed in 23 m/s air stream velocity and -3°C air temperature with two 45° and 90° angle of impact (Conditions 1 and 2 in Table 3 respectively). The results are reported in Table 5. For all three superhydrophobic coatings, less electrical heat input was required to maintain an ice-free surface compared to the uncoated sample. It is noteworthy that the SPS coating in both conditions requires the least amount of heat to maintain an ice-free surface. As discussed above, this can be attributed to the thickness of the coatings and the fact that the relatively thicker polymeric coatings act as a thermal barrier, requiring more power to increase the surface temperature to a level sufficient for preventing ice formation.

Table 5. Minimum electrical power required to maintain an ice-free surface at two angles of impact (AoI).

Sample	AoI = 90°		AoI = 45°	
	Power (W)	Improvement (%)	Power (W)	Improvement (%)
Uncoated	36	--	24	--
SPS	30	17	16	33
NW	33	8	20	17
UED	33	8	21	13

It must be noted that the use of thermally sprayed coatings with heating elements for dealing with in-flight and other types of icing has been previously reported. In a number of cases, metallic coatings have been deposited onto polymer substrates [56] to act as heating elements. For example Lopera-Valle et al. [57,58] reported using flame spray to deposit NiCrAlY coatings that showed promising results in terms of mitigating the ice accretion on structures exposed to cold environments. Atmospheric plasma spray (APS) has also been employed to generate FeCrAl heating elements. However, this study presents novel results in coupling heating of the coating and superhydrophobicity of the surface to mitigate the icing more efficiently.

It is important to note at this point that overall, we can see that superhydrophobic coatings can contribute to mitigating the icing by reducing ice accretion, reducing the deicing time and reducing the heat required to maintain an ice-free surface. The performance of the SPS coating in decreasing ice accretion is similar to the commercial spray superhydrophobic coatings. However, the SPS coating has lower deicing time and requires less heat input to maintain an ice-free surface compared to both commercial polymeric superhydrophobic coatings. This difference is mainly due to the thickness of the polymeric coatings which causes them to act as a barrier to

the heating from underneath the surface of the samples. Now that it has been established that the SPS coating performs positively in mitigating the icing and improving deicing, in the next sections its durability and mechanical performance are studied and compared to the commercial superhydrophobic coatings.

3.2. Durability Tests

3.2.1. Dry Particle Erosion Test

The first set of durability tests were designed to evaluate the dry particle erosion resistance of the superhydrophobic coatings. The change in wetting characteristics of the coatings after multiple iterations of the dry particle erosion test is shown in Figure 5.

According to Figure 5, the SPS coating shows significantly better durability in this test. The CA of the SPS coating does not change significantly even after five repetitions of this test. Furthermore, the SPS coating still shows a reasonable water mobility after five iterations of the test with a SA of below 10° and a CAH of below 20°. This is in contrast with both commercial coatings that quickly deteriorate and lose their superhydrophobic behavior after a few iterations of the test. Indeed, as shown in Figure 5, the CA of both commercial coatings drops to below 150° after two iterations. More importantly, both commercial coatings lose their water mobility (having CAH of more than 60°) and a water droplet pins on their surface i.e. no sliding occurs, after only one iteration.

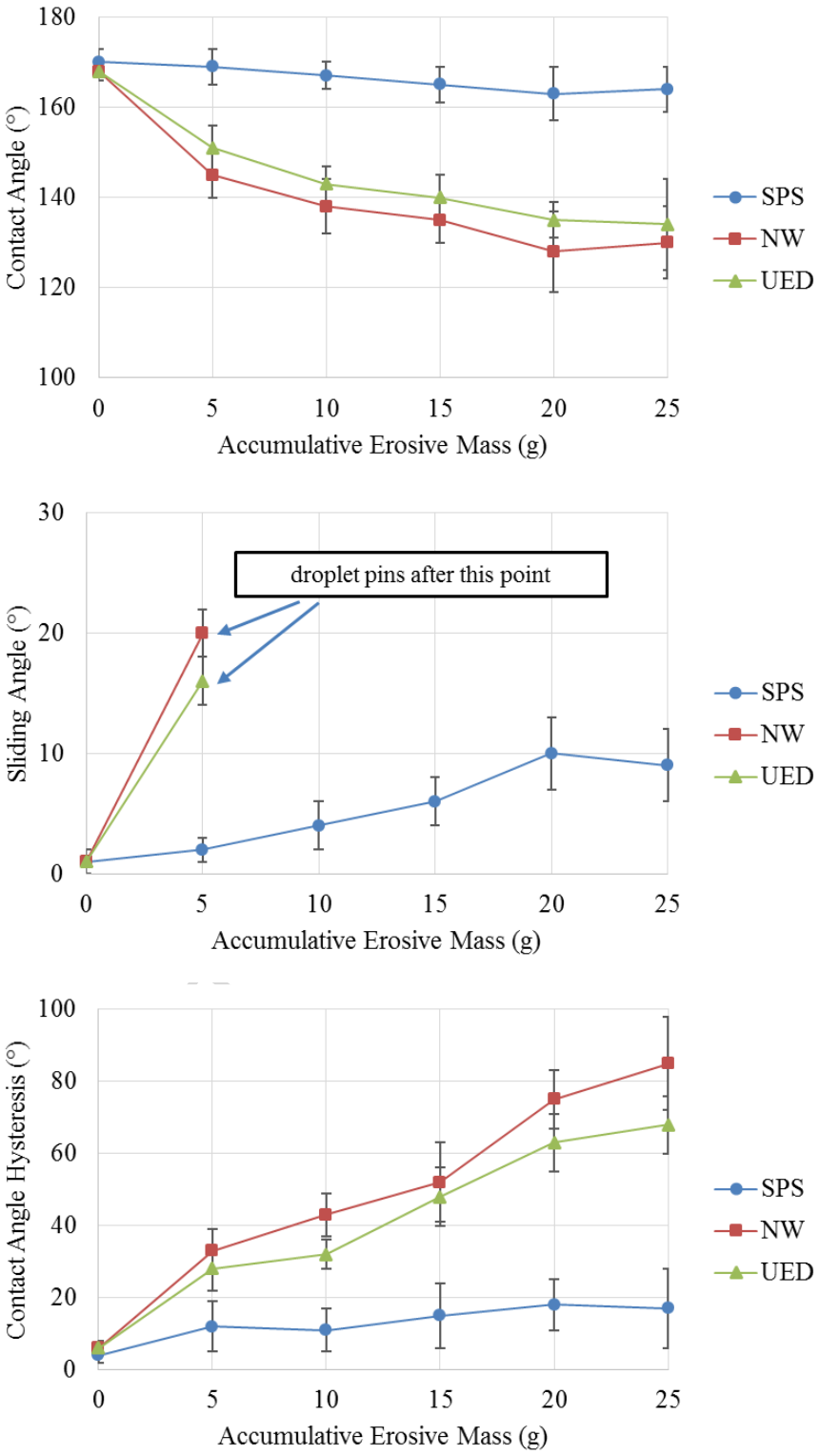

Figure 5. Change in CA, CAH and SA of different coating per accumulated mass of erosive particles [error bars represent standard deviation].

The significant difference between the SPS coating and the commercial polymer coatings in terms of dry particle erosion is due to the relatively soft nature of the polymeric coatings. This allows for the erosive particles to not only remove material from the surface of the coating and damage the coating microtexture, but also for especially smaller particles, to penetrate the coating and adhere to the surface. This penetration and embedding of small alumina particles in the polymeric coatings was observed using optical microscopy. These microscopic particles result in a rapid deterioration of superhydrophobic characteristic of the polymeric coatings. On the other hand, the SPS coating, made of TiO_2, is significantly harder and more resistant to penetration of abrasive particles. Thus, most abrasive particles are removed easily by the compressed air.

3.2.2. Cloud-Sized Water Droplet Erosion Test

In the next step of durability testing, the water droplet erosion resistance of the superhydrophobic coatings was evaluated. It worth noting that these droplets are five times larger in diameter than the droplets used in the icing test (i.e. MVD = 30μm). This droplet size is considerable larger than the water droplets that impact on the surfaces of the aircraft while passing through clouds in icing conditions. However, they can reasonably represent larger rain droplets that impact onto the aircraft surface in lower altitudes. As mentioned before, these droplets were characterized using the PDPA laser system which revealed their velocity to be close to 45 m/s just before the impact on the substrate. This velocity is roughly half of the velocity of a passenger aircraft when it passes through the clouds.

The change in CA, SA and CAH of the coatings after multiple iterations of the cloud-sized water droplet erosion test is shown in Figure 6. It is clear that out of the three samples, the UED commercial coating is more resistant to water droplet erosion. The change in wetting

characteristics of the SPS coating is very close to the NW commercial coating. The deterioration in superhydrophobic properties of the SPS coating occurs mainly due to gradual removal of the thin stearic acid layer from the surface which will be discussed further in the following paragraph. This stearic acid is extremely thin and transparent and therefore it is very difficult to give an exact value for its thickness.

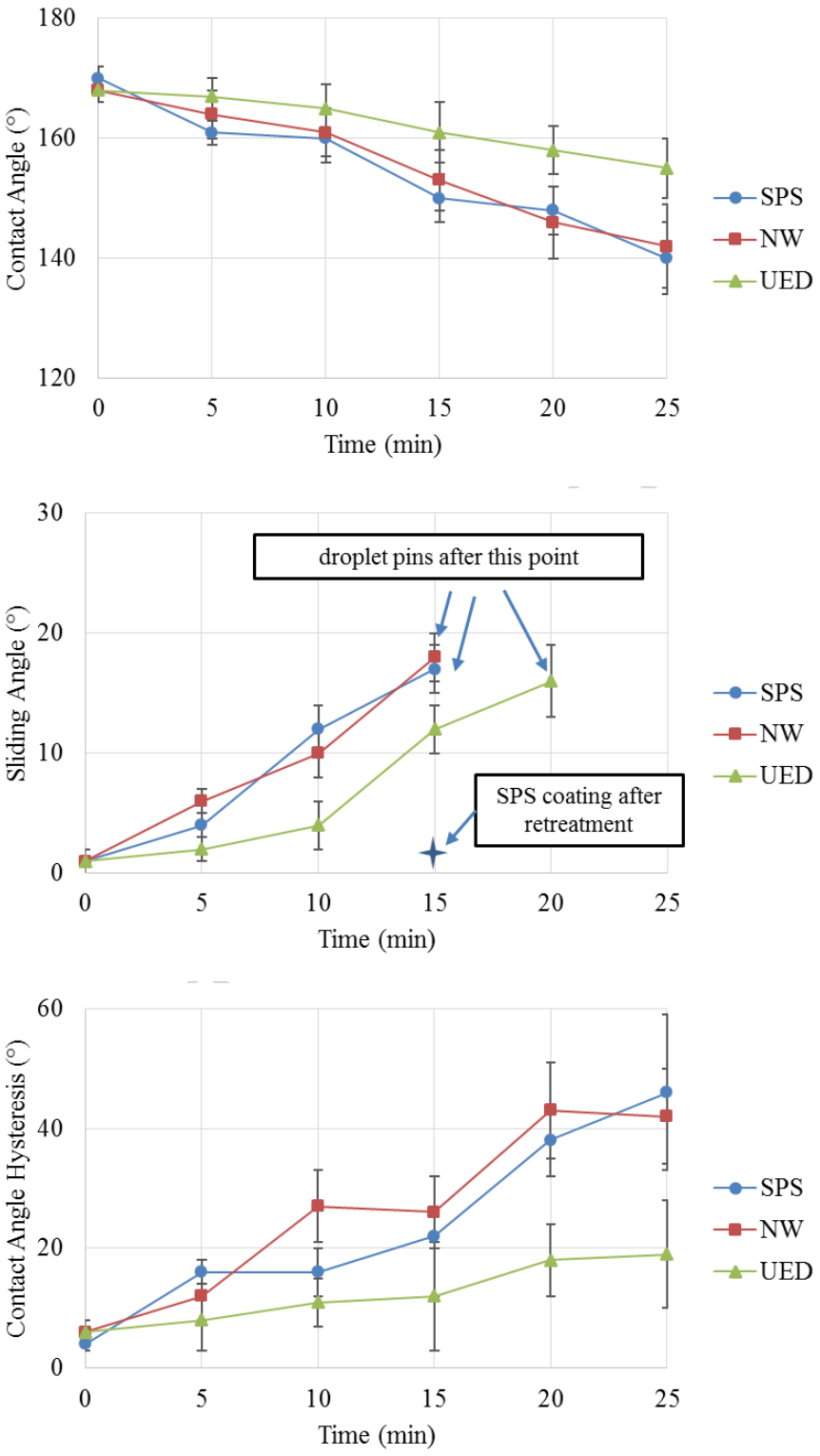

Figure 6. Change in CA, CAH and SA of different coatings per exposure time to 150 µm cloud-sized water droplet impacts at 45 m/s [error bars represent standard deviation].

There are two important points to consider regarding the cloud-sized water droplet erosion results. First, attempts to increase the thickness of the stearic acid treatment and consequently improving its durability can cause negative side effect since a relatively thick layer of stearic acid covers some of the hierarchical features of the coating micro-texture and results in reduced contact angle and water mobility of the coating. Second, an advantage of the SPS coating compared to the commercial coatings is that after the superhydrophobicity of the SPS coating has been reduced due to water erosion, a simple and quick retreatment by stearic acid solution immediately recovers the CA, SA and CAH to their initial values as demonstrated in Figure 6 This was experimentally demonstrated. This is in contrast to the commercial polymeric coatings where after the coatings are damaged, the surface needs to be cleaned of the remaining coating and then the coated again. This advantage is because while the stearic acid layer is removed by cloud-sized droplet erosion, the bulk of the TiO_2 base coating remains intact with its hierarchical micro-texture remaining unaffected by the water droplet erosion. On the contrary, when the wetting behavior of the commercial superhydrophobic coatings deteriorate, it is due to damage to the bulk of the coating.

To observe the effect of cloud-sized water droplet erosion on icing performance of the SPS coatings, the icing tests in conditions 1 and 8 of the Table 3 were repeated for the samples after exposure to this test. The results are reported in Figure 7, which indicate that after erosion, by losing their superhydrophobicity, the SPS coatings do not show any benefit in mitigating the ice accretion.

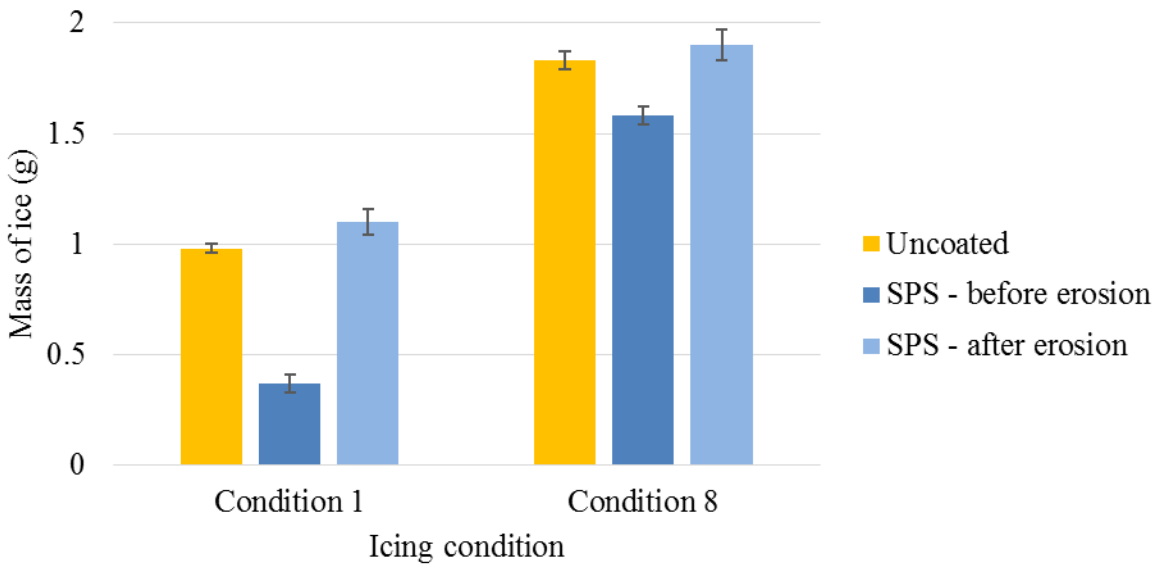

Figure 7. Ice accretion test comparison for uncoated sample versus the SPS, before and after cloud-sized water erosion test. (The error bars represent standard deviation)

3.2.3. High Intensity Water Erosion Test

To verify that the bulk of the SPS coating is more resistant to water droplet erosion, a high intensity water erosion test was designed and performed on all coatings. As detailed in Methodology section, this test was performed using a test setup specifically designed to test water erosion resistant coatings. Noting that even the mildest setting of this specific test was too erosive for the superhydrophobic coatings, this least intensive condition with MVD = 260 µm droplet size and 200 m/s droplet impact velocity was used.

The results of high intensity water erosion are demonstrated in Figure 8. It is also noteworthy that the shortest duration of test possible while having consistent and repeatable impact results was 5 seconds. As demonstrated in Figure 8, both commercial spray-on coatings failed completely even for this 5 second test i.e. the coatings were completely removed at the line of impact and the surface of the substrates were completely visible. The SPS coating lost its superhydrophobicity with its CA dropping to below 120°, no sliding and CAH increasing to

larger than 40° after the 5 second test. However, no considerable loss of coating mass was observed for the SPS coating after 5, 10 and 20 seconds of testing and the first considerable loss of mass which was approximately 3% occurred after 60 seconds of testing. After each step of this test, the SPS samples were retreated with stearic acid solution and their CA, SA and CAH was re-measured. It was observed that for the samples exposed to the erosion test up to 60 second, the superhydrophobic characteristics would completely recover after retreatment by stearic acid solution. The SPS samples that were exposed to the erosion test for longer than 60 seconds did not recover their original wetting values after retreatment and the coatings would show reduced water mobility. This was due to physical removal of coating material and damage to the hierarchical micro-texture of the coatings. Since the SPS coating are relatively thin and around 20 μm in thickness and the area impacted by the droplets in this test is relatively small (approximately 1 by 5 millimeters), the eroded mass of the coating is very small and therefore difficult to quantify. However in a qualitative analysis by SEM, it was discovered that the mass loss of the coating in exposure times up to 60 seconds is very insignificant. It is only in the next step and after 120 seconds that the coating demonstrates significant mass loss and therefore cannot be retreated to recover its superhydrophobicity.

SEM micrographs of the surface of the coating after 120, 300 and 600 seconds is demonstrated in Figure 8 (b), (c) and (d) consecutively. It can be seen in Figure 8 (b) that the cauliflower-like features of the coating are mainly removed in the initial stages of the coating erosion. Although at this point only around 20% of the mass of the coating has been removed, since the hierarchical micro-texture of the surface is lost, the coating cannot regain superhydrophobicity even after retreatment.

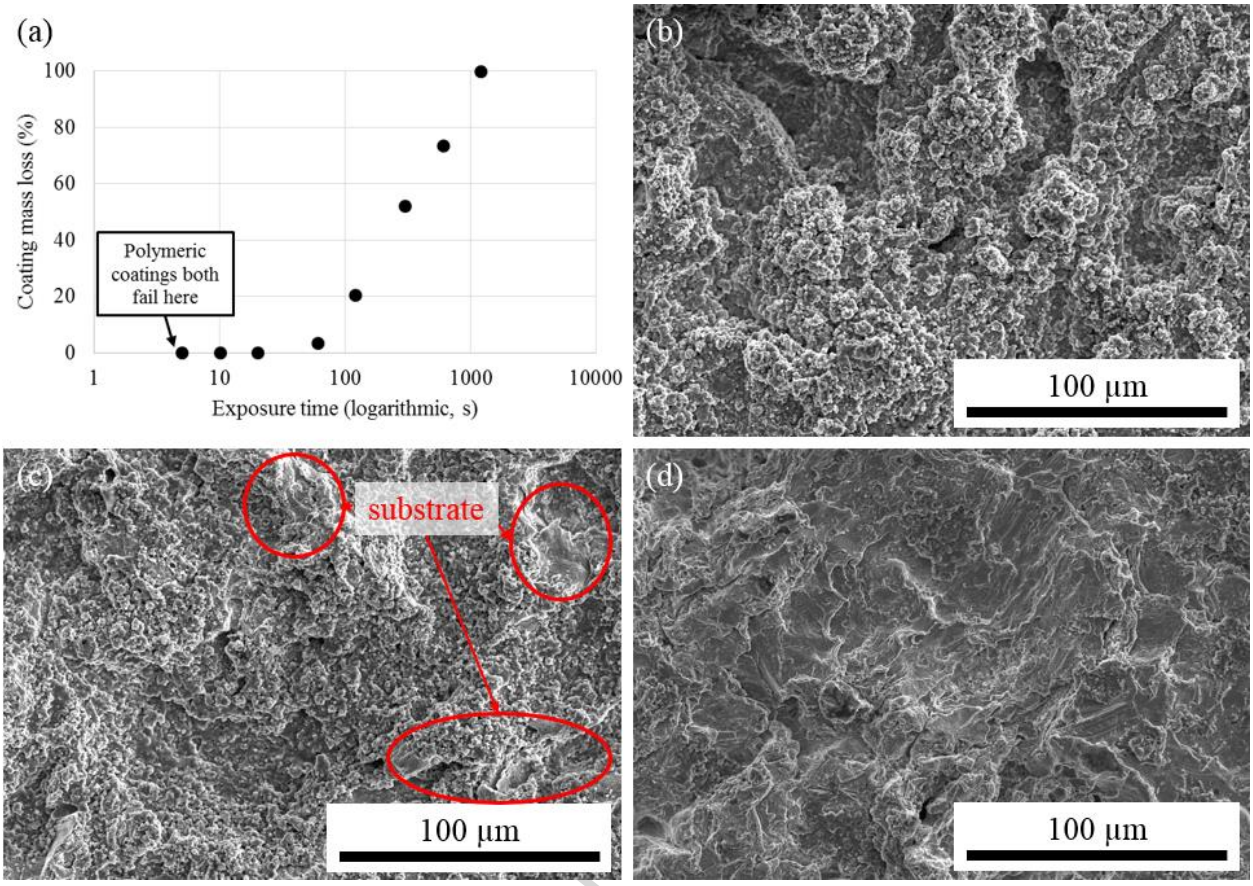

Figure 8. (a) Percent of coating material removed versus time in high intensity water erosion test. (b), (c) and (d) SEM micrographs of SPS coating after 120, 300 and 600 seconds, respectively.

In Figure 8 (c) it is observed that the bulk of the SPS coating is gradually removed and in some regions the steel substrate is visible after 300 seconds and more. In Figure 8 (d), mainly the substrate is visible and only small fractions of the coating material can be observed at some spots. As mentioned before the SPS coating remains almost completely intact after 20 seconds with the hierarchical micro-texture preserved and it loses only 3% of its mass after 60 seconds. On the other hand, complete failure of both commercial spray coatings occurs faster than the shortest testing duration which is 5 seconds. It can be concluded that the bulk of the SPS coating is at least an order of magnitude more resistance to water erosion in this test than the commercial superhydrophobic spray coatings.

3.2.4. Icing/Deicing Cyclic Test

The last test was designed to evaluate the durability of the superhydrophobic coatings to repeated cycles of icing and deicing. As detailed in methodology section, this test involved forming ice on the surface of the coatings in the wind tunnel for the duration of one minute, then deicing and drying using a heat gun. This cycle was carried out in groups of ten repetitions after which the wetting characteristics of the coating were re-evaluated. Changes in the wetting characteristics of the coatings after exposure to multiple cycles of icing/deicing are demonstrated in Figure 9. It was observed that the superhydrophobic characteristics of the polymeric commercial coatings deteriorate quite rapidly after being exposed to multiple icing and deicing cycles. In fact, both NW and UED coatings show a quick drop in CA value and a sharp increase in SA and CA hysteresis after 10 icing/deicing cycles.

In contrast, the SPS superhydrophobic coating shows almost no significant deterioration of properties after 40 icing/deicing cycles. The main contributor to this significantly different behavior can be the fact that as water droplets freeze on the surface of the polymeric coatings, the change of volume of the ice causes damage to the surface of the relatively soft polymeric coatings. On the other hand, the SPS TiO_2 coating's micro-texture remains unaffected due to the higher hardness and stiffness of TiO_2. It is noteworthy that no significant change in the ice accretion was observed in the SPS coatings after 40 icing/deicing cycles.

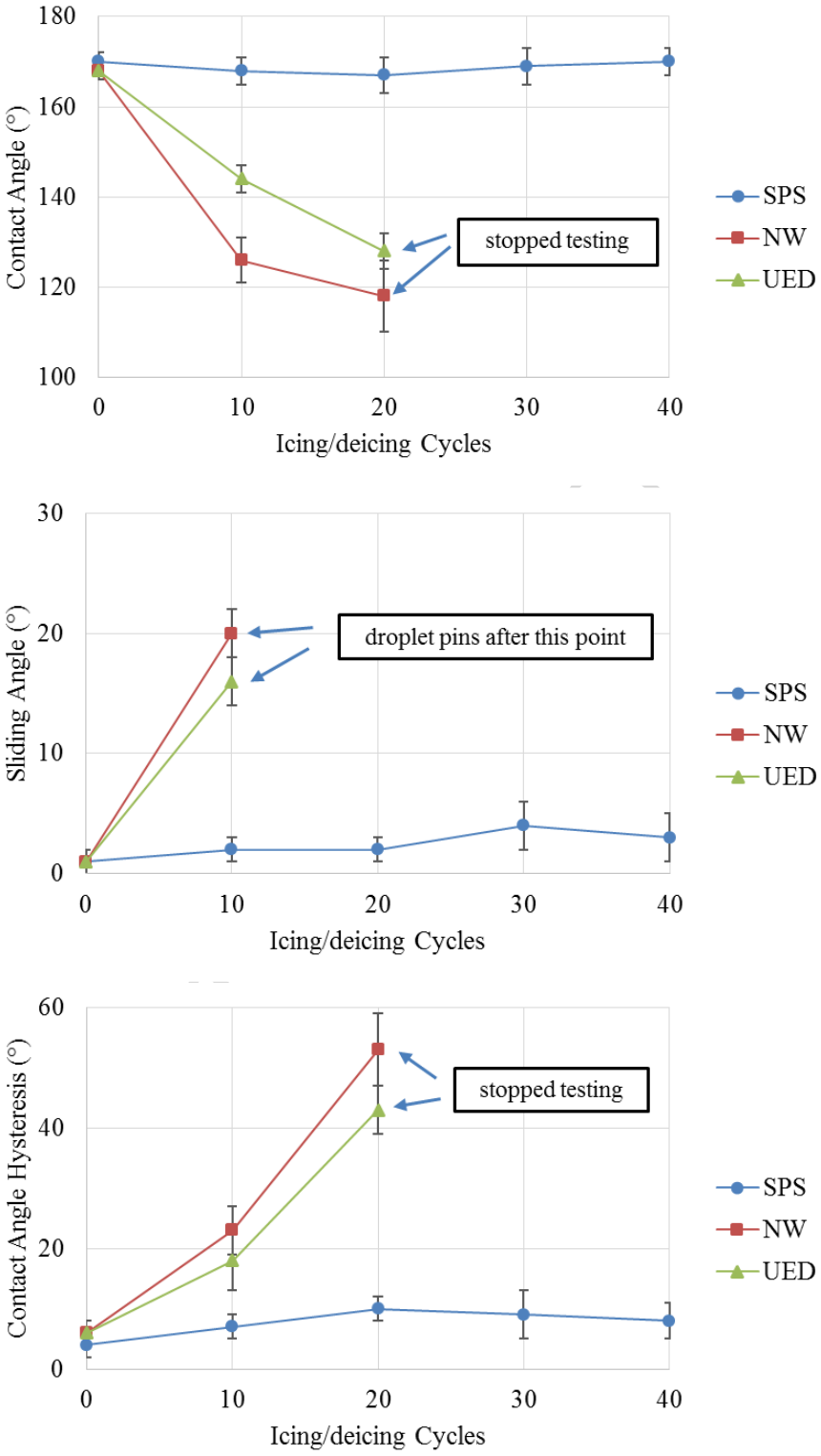

Figure 9. Change in SA and CAH of samples after multiple icing/deicing cycles [error bars represent standard deviation].

The SPS TiO_2 superhydrophobic coating has an R_a of 8.5± 0.3 µm and an R_z of 82 ± 3 µm. No significant change in the roughness of the coating was observed after the cloud-sized water erosion test and icing-deicing cycle. On the other hand, after the high intensity water erosion test, the roughness of the coating certainly changes as there is evident alteration in the microtexture of the coating. However, this change cannot be quantified as the impacted area in this tests is very narrow which makes it challenging to measure the roughness in a consistent and reliable manner.

It was observed in the durability tests that the SPS coating is considerably more resistant to dry particle erosion and cyclic icing/deicing in comparison to both commercial superhydrophobic coatings. While in both of these tests the SPS coating preserves its superhydrophobic properties, the commercial coatings lose their properties and become sticky. Regarding the water erosion cloud-sized droplet test, it was demonstrated that the SPS coating performs similar to the NW commercial coatings while the UED commercial coating showed somewhat more resistance. However, it was demonstrated that the SPS coating has an advantage in terms of reparability. This is because the hierarchical micro-texture of the SPS TiO_2 remains intact and is at least an order of magnitude more erosion resistant compared to the bulk of the commercial coatings when tested in high intensity erosion resistance tests. As long as the hierarchical micro-textured TiO_2 is preserved, the coating can be simply re-treated with the stearic acid solution to regain its superhydrophobicity. This is in contrast to the commercial polymeric coating that if damaged, need to be completely removed, cleaned and recoated.

4. Summary and Conclusions

In this work, a superhydrophobic coating was prepared by suspension plasma spraying (SPS) of a TiO2 feedstock suspension onto grit-blasted substrates to generate a hierarchically

micro-textured surface. The coating was then treated with a solution of stearic acid to lower its surface energy which resulted in superhydrophobic behavior with a contact angle (CA) as high as 170°, a sliding angle (SA) of 1° and a contact angle hysteresis of 4°. This coating was tested to evaluate its potential performance in mitigating in-flight icing under simulated icing conditions in a wind tunnel. The results are then compared to two different commercial, polymer-based superhydrophobic spray coatings. Additionally, since durability and especially erosion resistance are a major challenge in preparing superhydrophobic coatings for practical applications and more specifically anti-icing for aircraft; these coatings are tested for their erosion resistance and cyclic icing/deicing durability.

Regarding the icing tests, it is found that the SPS coatings has a positive effect in decreasing the ice accretion and its performance in this case is similar to the performance of commercial superhydrophobic coating. However, in terms of facilitating heated deicing using an electrical heater placed under the samples, the SPS coating decreases both the deicing time and the electrical power required to maintain an ice-free surface more than the commercial coatings. This is mainly attributed to the fact that the commercial polymeric coatings are relatively thick and act as a barrier to heat transfer as opposed to the relatively thin SPS coating which significantly reduces this effect.

Regarding the durability tests, the SPS superhydrophobic coating demonstrated significantly better resistance to dry particle erosion compared to the two commercial coatings. This is due to the fact that the commercial polymer coatings are relatively soft and permit the sharp microscopic abrasive particles to penetrate into and adhere to the surface, causing a rapid deterioration of superhydrophobic behavior. On the other hand, the SPS coating is significantly more resistant to penetration and damage by abrasive particles due to the harder and stiffer TiO_2

ceramic. Furthermore, the SPS coatings also show significantly more durability after being exposed to multiple icing/deicing cycles. This considerable difference is once more attributed to the softer nature of polymer coatings compared to the harder and stiffer SPS TiO_2 coatings.

In terms of cloud-sized water droplet erosion, the SPS coating shows a behavior similar to one of the commercial coatings, the NeverWet (NW), while the other commercial coating, UltraEver Dry (UED) demonstrates slightly better resistance to water droplet erosion. However, it is very important to note that the SPS superhydrophobic coating present a potentially beneficial feature compared to both commercial coatings due to the fact that the hierarchical micro-texture and the bulk of the SPS coating remain intact after being exposed to extended water droplet erosion. This permits a quick and easy recovery of superhydrophobicity of the SPS coating using a simple retreatment with the stearic acid solution. This is in contrast to the commercial polymeric coating which, if damaged, requires complete removal, cleaning and recoating to be used again. The durability of the hierarchical micro-texture of the SPS TiO_2 is demonstrated through a high intensity water erosion test. In this test, the SPS coating was shown to be at least one order of magnitude more durable in intensive water erosion. The collection of the results and conclusions presented here suggest that the SPS superhydrophobic coatings could be a very efficient and rather durable candidate to be used for anti-icing protection on aircraft.

Acknowledgement

The authors with to thank Dr. Mohammad Sadegh Mahdipoor, Mr. Hani Jazaerli and Mr. Marc Roche for their support. This work was financially supported by Natural Science and Engineering Research Council of Canada (NSERC) and Consortium for Aerospace Research and Innovation in Canada (CARIC) through Canada and EU partnership project Phobic2Ice. This research was undertaken, in part, thanks to funding from the Canada Research Chairs Program.

References:

[1] W.J. Baars, R.O. Stearman, C.E. Tinney, A review on the impact of icing on aircraft stability and control., J. Aeroelasticity …. 2 (2010) 35–52. doi:10.3293/asdj.2010.7.

[2] M.K. Politovich, Response of a research aircraft to icing and evaluation of severity indices, J. Aircr. 33 (1996) 291–297. doi:10.2514/3.46936.

[3] C. Antonini, M. Innocenti, T. Horn, M. Marengo, A. Amirfazli, Understanding the effect of superhydrophobic coatings on energy reduction in anti-icing systems, Cold Reg. Sci. Technol. 67 (2011) 58–67. doi:10.1016/j.coldregions.2011.02.006.

[4] M.. Bragg, G.M. Gregorek, J.D. Lee, Airfoil Aerodynamics in Icing Conditions, J. Aircr. 23 (1985) 76–81. doi:10.2514/3.45269.

[5] G. Mingione, M. Barocco, E. Denti, F.G. Bindi, Flight in Icing Condition, Tech. Rep., 1997. http://www2.developpement-durable.gouv.fr/IMG/pdf/DGAC_Icing_flight_manual.pdf (accessed October 27, 2017).

[6] F. Caliskan, C. Hajiyev, A review of in-flight detection and identification of aircraft icing and reconfigurable control, Prog. Aerosp. Sci. 60 (2013) 12–34. doi:10.1016/j.paerosci.2012.11.001.

[7] J. Hallett, G. Isaac, M. Politovich, D. Marcotte, A. Reehorst, C. Ryerson, Alliance Icing Research Study II (AIRS II) Science Plan, 2003. http://citeseerx.ist.psu.edu/viewdoc/download?doi=10.1.1.575.298&rep=rep1&type=pdf (accessed November 8, 2017).

[8] E.J.Y. Ling, V. Uong, J.S. Renault-Crispo, A.M. Kietzig, P. Servio, Reducing Ice Adhesion on Nonsmooth Metallic Surfaces: Wettability and Topography Effects, ACS Appl. Mater. Interfaces. 8 (2016) 8789–8800. doi:10.1021/acsami.6b00187.

[9] S. Bengaluru Subramanyam, V. Kondrashov, J. Rühe, K.K. Varanasi, Low Ice Adhesion on Nano-Textured Superhydrophobic Surfaces under Supersaturated Conditions, ACS Appl. Mater. Interfaces. 8 (2016) 12583–12587. doi:10.1021/acsami.6b01133.

[10] M.K. Politovich, Aircraft Icing Caused by Large Supercooled Droplets, J. Appl. Meteorol. 28 (1989) 856–868. doi:10.1175/1520-0450(1989)028<0856:AICBLS>2.0.CO;2.

[11] S.G. Cober, G.A. Isaac, J.W. Strapp, Characterizations of Aircraft Icing Environments that Include Supercooled Large Drops, J. Appl. Meteorol. 40 (2001) 1984–2002.

http://journals.ametsoc.org/doi/pdf/10.1175/1520-0450%282001%29040%3C1984%3ACOAIET%3E2.0.CO%3B2 (accessed November 10, 2017).

[12] A. Reehorst, J. Chung, M. Potapczuk, Y. Choo, Study of Icing Effects on Performance and Controllability of an Accident Aircraft, J. Aircr. 37 (2000). doi:10.2514/2.2588.

[13] M.K. Politovich, Predicting Glaze or Rime Ice Growth on Airfoils, J. Aircr. 37 (2000) 117–122. doi:10.2514/2.2570.

[14] T. Cebeci, F. Kafyeke, Aircraft Icing, Annu. Rev. Fluid Mech. 35 (2003) 11–21. doi:10.1146/annurev.fluid.35.101101.161217.

[15] Pilot Guide: Flight in Icing Condition, 2015. https://www.faa.gov/documentLibrary/media/Advisory_Circular/AC_91-74B.pdf (accessed October 30, 2017).

[16] M.B. Bragg, T. Basar, W.R. Perkins, M.S. Selig, P.G. Voulgaris, J.W. Melody, N.B. Sarter, by M. B Bragg, T. Basar, W.R. Perkins, M.S. Selig, P. Voulgaris, J.W. Melody, Smart Icing Systems for Aircraft Icing Safety, AIAA Pap. 813 (2002). http://sis.ae.illinois.edu/papers/SISJofADraft02.pdf (accessed November 10, 2017).

[17] A. Lampton, J. Valasek, Prediction of icing effects on the lateral/directional stability and control of light airplanes, Aerosp. Sci. Technol. 23 (2012) 305–311. doi:10.1016/j.ast.2011.08.005.

[18] G.A. Isaac, S.G. Cober, J.W. Strapp, A.V. Korolev, A. Tremblay, D.L. Marcotte, Recent Canadian Research on Aircraft In-Flight Icing, Can. Aeronaut. Sp. J. 47 (2001) 213–221. https://www.researchgate.net/profile/A_Korolev/publication/257240101_Recent_Canadian_Research_on_Aircraft_In-Flight_Icing/links/00b7d524c119432719000000.pdf (accessed October 27, 2017).

[19] Y. Wang, J. Xue, Q. Wang, Q. Chen, J. Ding, Verification of icephobic/anti-icing properties of a superhydrophobic surface, ACS Appl. Mater. Interfaces. 5 (2013) 3370–3381. doi:10.1021/am400429q.

[20] D.K. Sarkar, M. Farzaneh, Superhydrophobic Coatings with Reduced Ice Adhesion, J. Adhes. Sci. Technol. 23 (2009) 1215–1237. doi:10.1163/156856109X433964.

[21] L.B. Boinovich, A.M. Emelyanenko, Anti-icing potential of superhydrophobic coatings, Mendeleev Commun. 23 (2013) 3–10. doi:10.1016/j.mencom.2013.01.002.

[22] A. Lafuma, D. Quéré, Superhydrophobic states, Nat. Mater. 2 (2003) 457–460. doi:10.1038/nmat924.

[23] J.B. Boreyko, C.H. Baker, C.R. Poley, C.H. Chen, Wetting and dewetting transitions on hierarchical superhydrophobic surfaces, Langmuir. 27 (2011) 7502–7509. doi:10.1021/la201587u.

[24] G. Momen, R. Jafari, M. Farzaneh, Ice repellency behaviour of superhydrophobic surfaces: Effects of atmospheric icing conditions and surface roughness, Appl. Surf. Sci. 349 (2015) 211–218. doi:10.1016/j.apsusc.2015.04.180.

[25] S. Zheng, C. Li, Q. Fu, W. Hu, T. Xiang, Q. Wang, M. Du, X. Liu, Z. Chen, Development of stable superhydrophobic coatings on aluminum surface for corrosion-resistant, self-cleaning, and anti-icing applications, Mater. Des. 93 (2016) 261–270. doi:10.1016/j.matdes.2015.12.155.

[26] C. Lee, C.J. Kim, Underwater restoration and retention of gases on superhydrophobic surfaces for drag reduction, Phys. Rev. Lett. 106 (2011) 1–4. doi:10.1103/PhysRevLett.106.014502.

[27] C. Chen, Q. Cai, C. Tsai, C.-L. Chen, G. Xiong, Y. Yu, Z. Ren, Dropwise condensation on superhydrophobic surfaces with two-tier roughness, Appl. Phys. Lett. 90 (2007) 1–4. doi:10.1063/1.2731434.

[28] P. Zhang, F.Y. Lv, A review of the recent advances in superhydrophobic surfaces and the emerging energy-related applications, Energy. 82 (2015) 1068–1087. doi:10.1016/j.energy.2015.01.061.

[29] P. Tourkine, M. Le Merrer, D. Quéré, Delayed freezing on water repellent materials, Langmuir. 25 (2009) 7214–7216. doi:10.1021/la900929u.

[30] G. Fang, A. Amirfazli, Understanding the anti-icing behavior of superhydrophobic surfaces, Surf. Innov. 2 (2014) 94–102. doi:10.1680/si.13.00046.

[31] R. Liao, Z. Zuo, C. Guo, Y. Yuan, A. Zhuang, Fabrication of superhydrophobic surface on aluminum by continuous chemical etching and its anti-icing property, Appl. Surf. Sci. 317 (2014) 701–709. doi:10.1016/j.apsusc.2014.08.187.

[32] Z.J. Wang, D.J. Kwon, K. Lawrence DeVries, J.M. Park, Frost formation and anti-icing performance of a hydrophobic coating on aluminum, Exp. Therm. Fluid Sci. 60 (2015) 132–137. doi:10.1016/j.expthermflusci.2014.09.003.

[33] K.K. Varanasi, T. Deng, J.D. Smith, M. Hsu, N. Bhate, Frost formation and ice adhesion on superhydrophobic surfaces, Appl. Phys. Lett. 97 (2010) 234102. doi:10.1063/1.3524513.

[34] C. Laforte, A. Beisswenger, Icephobic Material Centrifuge Adhesion Test, Proc. Int. Work. Atmos. Icing Struct. (IWAIS XI). (2005) 1–5. http://www.mendeley.com/research/icephobic-material-centrifuge-adhesion-test/.

[35] J. Chen, J. Liu, M. He, K. Li, D. Cui, Q. Zhang, X. Zeng, Y. Zhang, J. Wang, Y. Song, Superhydrophobic surfaces cannot reduce ice adhesion, Appl. Phys. Lett. 101 (2012) 111603. doi:10.1063/1.4752436.

[36] I. Malavasi, I. Bernagozzi, C. Antonini, M. Marengo, Assessing durability of superhydrophobic surfaces, Surf. Innov. 3 (2014) 49–60. doi:10.1680/si.14.00001.

[37] A. Milionis, E. Loth, I.S. Bayer, Recent advances in the mechanical durability of superhydrophobic materials, Adv. Colloid Interface Sci. 229 (2016) 57–79. doi:10.1016/j.cis.2015.12.007.

[38] P. Juuti, J. Haapanen, C. Stenroos, H. Niemelä-Anttonen, J. Harra, H. Koivuluoto, H. Teisala, J. Lahti, M. Tuominen, J. Kuusipalo, P. Vuoristo, J.M. Mäkelä, Achieving a slippery, liquid-infused porous surface with anti-icing properties by direct deposition of flame synthesized aerosol nanoparticles on a thermally fragile substrate, Appl. Phys. Lett. 110 (2017) 161603. doi:10.1063/1.4981905.

[39] H. Koivuluoto, C. Stenroos, M. Kylmälahti, M. Apostol, J. Kiilakoski, P. Vuoristo, Anti-icing Behavior of Thermally Sprayed Polymer Coatings, J. Therm. Spray Technol. 26 (2016) 150–160. doi:10.1007/s11666-016-0501-x.

[40] N. Sharifi, M. Pugh, C. Moreau, A. Dolatabadi, Developing hydrophobic and superhydrophobic TiO2 coatings by plasma spraying, Surf. Coatings Technol. (2016). doi:10.1016/j.surfcoat.2016.01.029.

[41] N. Sharifi, F. Ben Ettouil, C. Moreau, A. Dolatabadi, M. Pugh, Engineering surface texture and hierarchical morphology of suspension plasma sprayed TiO 2 coatings to control wetting behavior and superhydrophobic properties, Surf. Coatings Technol. 329 (2017) 139–148. doi:10.1016/j.surfcoat.2017.09.034.

[42] N. Czernkovich, Understanding in-flight icing, in: Transp. Canada Aviat. Saf. Semin., Citeseer, 2004: pp. 1–21.

[43] D. De Pauw, A. Dolatabadi, Effect of Superhydrophobic Coating on the Anti-Icing and Deicing of an Airfoil, J. Aircr. 54 (2017) 490–499. doi:10.2514/1.C033828.

[44] A.F. Stalder, G. Kulik, D. Sage, L. Barbieri, P. Hoffmann, A snake-based approach to accurate determination of both contact points and contact angles, Colloids Surfaces A Physicochem. Eng. Asp. 286 (2006) 92–103. doi:10.1016/j.colsurfa.2006.03.008.

[45] A.F. Stalder, T. Melchior, M. Müller, D. Sage, T. Blu, M. Unser, Low-bond axisymmetric drop shape analysis for surface tension and contact angle measurements of sessile drops, Colloids Surfaces A Physicochem. Eng. Asp. 364 (2010) 72–81. doi:10.1016/j.colsurfa.2010.04.040.

[46] L. Xu, D. Zhu, X. Lu, Q. Lu, Transparent, thermally and mechanically stable superhydrophobic coating prepared by an electrochemical template strategy, (n.d.). doi:10.1039/c4ta06944g.

[47] X. Deng, L. Mammen, Y. Zhao, P. Lellig, K. Müllen, C. Li, H.J. Butt, D. Vollmer, Transparent, thermally stable and mechanically robust superhydrophobic surfaces made from porous silica capsules, Adv. Mater. 23 (2011) 2962–2965. doi:10.1002/adma.201100410.

[48] X. Deng, L. Mammen, H.-J. Butt, D. Vollmer, Candle Soot as a Template for a Transparent Robust Superamphiphobic Coating, Science (80-.). 335 (2012) 67 LP-70. http://science.sciencemag.org/content/335/6064/67.abstract.

[49] A. Standard, G73, 2010, Standard test method for liquid impingement erosion using rotating apparatus, (2010).

[50] M.S. Mahdipoor, F. Tarasi, C. Moreau, A. Dolatabadi, M. Medraj, HVOF sprayed coatings of nano-agglomerated tungsten-carbide/cobalt powders for water droplet erosion application, Wear. 330–331 (2015) 338–347. doi:10.1016/j.wear.2015.02.034.

[51] M.S. Mahdipoor, D. Kevorkov, P. Jedrzejowski, M. Medraj, Water droplet erosion mechanism of nearly fully-lamellar gamma TiAl alloy, Mater. Des. 89 (2016) 1095–1106. doi:10.1016/j.matdes.2015.10.077.

[52] M.K. Politovich, Predicting In-Flight Aircraft Icing Intensity, J. Aircr. 40 (2003) 639–644. doi:10.2514/2.3167.

[53] U. Diebold, The surface science of titanium dioxide, Surf. Sci. Rep. 48 (2003) 53–229. doi:10.1016/S0167-5729(02)00100-0.

[54] P. Fauchais, R. Etchart-Salas, V. Rat, J.F. Coudert, N. Caron, K. Wittmann-Ténèze, Parameters controlling liquid plasma spraying: Solutions, sols, or suspensions, J. Therm. Spray Technol. 17 (2008) 31–59. doi:10.1007/s11666-007-9152-2.

[55] C.L. Choy, Thermal conductivity of polymers, Polymer (Guildf). 18 (1977) 984–1004. doi:10.1016/0032-3861(77)90002-7.

[56] R. Gonzalez, H. Ashrafizadeh, A. Lopera, P. Mertiny, A. McDonald, A Review of Thermal Spray Metallization of Polymer-Based Structures, J. Therm. Spray Technol. 25 (2016) 897–919. doi:10.1007/s11666-016-0415-7.

[57] A. Lopera-Valle, A. McDonald, Flame-sprayed coatings as de-icing elements for fiber-reinforced polymer composite structures: Modeling and experimentation, Int. J. Heat Mass Transf. 97 (2016) 56–65. doi:10.1016/J.IJHEATMASSTRANSFER.2016.01.079.

[58] A. Lopera-Valle, A. McDonald, Application of Flame-Sprayed Coatings as Heating Elements for Polymer-Based Composite Structures, J. Therm. Spray Technol. 24 (2015) 1289–1301. doi:10.1007/s11666-015-0302-7.

Highlights

- Reduced ice accretion on superhydrophobic coatings
- Combining heating and use of superhydrophobic coatings to mitigate in-flight icing
- Promising coating durability against particle erosion and icing-deicing cycles